Review

Lead-Free Halide Double Perovskite for High-Performance Photodetectors: Progress and Perspective

Xiaoyan Li , Junzhe Shi , Jianjun Chen , Zuojun Tan * , Hongwei Lei *

Posted Date: 28 April 2023

doi: 10.20944/preprints202304.1145.v1

Keywords: Lead-free; Double perovskite; Photodetector doi:10.20944/preprints202304.1145.v1

Article

Lead-Free Halide Double Perovskite for High-Performance Photodetectors: Progress and Perspective

Xiaoyan Li, Junzhe Shi, Jianjun Chen, Zuojun Tan * and Hongwei Lei *

College of Engineering, Huazhong Agricultural University, Wuhan, 430070, China
* Correspondence: tzj@mail.hzau.edu.cn, leihw@mail.hzau.edu.cn

Abstract: Lead halide perovskite has become a promising candidate for high-performance photodetector (PD) applications due to its attractive optical and electrical properties such as high optical absorption coefficient, high carrier mobility, and long carrier diffusion length. However, the presence of highly toxic lead in these devices has limited their practical applications and even hindered their progress toward commercialization. Therefore, the scientific community has been committed to searching for low-toxic and stable perovskite-type alternative materials. Lead-free double perovskite materials, which are still in the preliminary stage of exploration, have achieved inspiring results in recent years. In this review, we mainly focused on two types of lead-free double perovskite based on different Pb substitution strategies, including $A_2M(I)M(III)X_6$ and $A_2M(IV)X_6$. We reviewed the research progress and prospects of lead-free double perovskite photodetectors in the past three years. And more importantly, from the perspective of optimizing inherent defects in materials and improving device performance, we proposed some feasible pathways and made an encouraging perspective for the future development of lead-free double perovskite photodetectors.

Keywords: Lead-free; Double perovskite; Photodetector

---

1. Introduction

Lead halide perovskite has the advantages of a direct band gap, large absorption coefficient, long carrier lifetime, low defect density[1], and high solution processability, making it a good candidate for optoelectronic applications. As one of the most important optoelectric devices, lead halide perovskite photodetectors have recently attracted enormous attention because of their potential application in optical communications, medical near-infrared imaging, military surveillance, and chemical/biological sensing. Despite the amazing achievements of lead-based photodetectors, the toxicity and chronic degradation of Pb to the human central nervous system and ecosystem cannot be underestimated[2], which has gradually become a major resistance to the commercialization of lead-based photodetectors. Therefore, it is necessary to explore intrinsically stable and environmentally friendly inorganic lead-free perovskite, which is conducive to future commercial development and is also the focus of researchers.

Among all the lead-free perovskite materials, lead-free double perovskite has emerged as a very promising candidate to address both the stability and toxicity issues in lead-based perovskites. Theoretically, lead-free double perovskite can be designed and synthesized by replacing Pb^{2+} with a low- or non-toxic metal ion. To maintain charge neutrality, two Pb^{2+} cations can usually be replaced by one monovalent metal cation M(I) and a trivalent metal cation M(III) to form the double perovskite with a general formula of $A_2M(I)M(III)X_6$, where M(I)=Na^+, K^+, Rb^+, Cu^+, Ag^+, Au^+, In^+, and Tl^+, and M(III)=Bi^{3+}, Sb^{3+}, In^{3+}, Au^{3+}, Tl^{3+}, and Fe^{3+}. Two Pb^{2+} ions can also be replaced by one tetravalent metal cation M(IV) to form the vacancy-ordered double perovskite with a general formula of $A_2M(IV)X_6$, where A=MA^+, FA^+, and Cs^+, M(IV)= Sn^{4+}, Ge^{4+}, Ti^{4+}, Pd^{4+}, Hf^{4+}, Te^{4+}, Zr^{4+}, and Cr^{4+}, and X=Cl^-, Br^-, and I^-. In this review, we discuss the properties of lead-free double perovskite materials and highlight the outstanding advances concerning lead-free double perovskite photodetectors in the last three years. Then, we emphasize the limitations of lead-free perovskite photodetector materials and devices, followed by giving a comment on the possible solutions to solve the challenges and providing an inspiring outlook on their future directions.

2. Categories and Key Performance Parameters of Semiconductor-Based PDs

Semiconductor photodetectors are mainly divided into three categories according to their structures: photodiodes, photoconductors, and phototransistors. The structures of various types of detectors are shown in Figure 1. Photodiodes have narrow charge transit distance and inner electric field, thus they usually have fast response speed, low noise, and large detectivity, but suffer from low responsivity and EQE. As a contract, photoconductors have large responsivity/EQE because of the photoconductive gain but usually show low response time and small detectivity. Phototransistors would present balanced parameters among these three structures. The key performance parameters used to characterize photodetectors are the Responsivity (R), Detectivity (D^*), Response time (rise/decay time), On-off ratio, EQE, LDR, and their definitions are expressed as follows:

1. Responsivity (R): It is a key parameter to quantify the response efficiency of photodetectors to an optical signal and is defined as the photocurrent generated by the incident light of the unit power per unit area. Its unit is A W^{-1}.

$$R = \frac{I_{light} - I_{dark}}{P_{hv} S}$$

Where I_{light} is the light current generated by the light detector, I_{dark} is the dark current, P_{hv} is the incident light intensity, and S is the effective light area.

2. Detectivity (D^*): It describes the ability of detector materials to detect weak light. D^* is determined by the responsivity and noise of the PD and is defined as follows:

$$D^* = \frac{(S\Delta f)^{1/2}}{I_{noise}}$$

Where S is the effective light area of the detector, Δf is the electrical bandwidth, I_{noise} is the total noise current of the detector. Its unit is cm $Hz^{1/2}W^{-1}$.

3. Response time (rise/decay time): Response time reflects the response speed of the detector and is a key parameter to evaluate the performance of PDs. Generally, we can use the square wave test method to measure the optical response time of the detector. Where rise time (τr)/decay time (τf) is defined as the rise (fall) time from 10% (90%) to 90% (10%) of the maximum current, respectively. Its unit is s.
4. On-off ratio: The On-off ratio is the ratio of the photocurrent (Ip) and the dark current (Id), reflecting the photosensitivity of PDs. The higher the on-off current ratio, the higher the accuracy of the detector in detecting weak light signals.
5. EQE: It is defined as the ratio of output carriers to the number of incident photons per unit time under specific wavelength radiation, which reflects the luminous efficiency of the whole detector.

$$EQE = \frac{N_C}{N_I} = \frac{hc}{e\lambda} R$$

Where h is the Planck constant, c is the light velocity, e is the electronic charge， and λ is the wavelength of the incident light. Its unit is %.

LDR: It describes the region where the generated photocurrent is linearly dependent on the incident light intensity. Beyond this range, the intensity of the light signal cannot be detected and calculated precisely. Its unit is dB.

$$LDR = 20 \log \frac{{I_p}^*}{I_{dark}}$$

Where I_p^* is the photocurrent tested under a light intensity of 1 mW cm^{-2}.

doi:10.20944/preprints202304.1145.v1

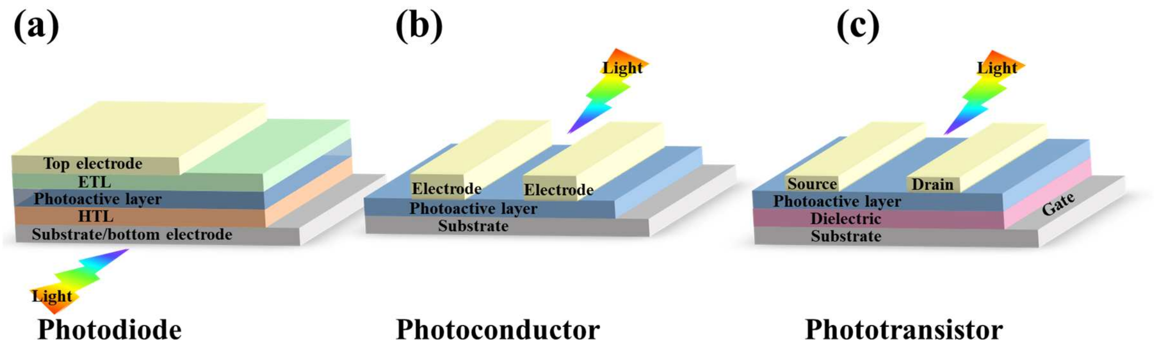

Figure 1. Schematic of architectures for different photodetectors.

3. Design Principle for Lead-Free Double Perovskite Materials

The crystal structure of lead-based halide perovskite with the general formula $APbX_3$ is shown in Figure 2a, where Pb^{2+} is bonded with six X halide ions ($X=I^-$, Br^- and Cl^-) to form $[PbX_6]^{4-}$ with an octahedral structure, and each $[PbX_6]^{4-}$ octahedron is connected by an angle sharing mode, thus forming a 3D frame. The A-site cation including methylammonium (MA^+), formamidinium (FA^+), and Cs^+ with large ion radius, is filled in the octahedral cavity to maintain the stability of the 3D structure. To avoid the use of toxic Pb elements, two effective strategies for replacing Pb^{2+} ions were investigated. One strategy is to replace two Pb^{2+} ions with two heterovalent metal ions to form a double perovskite with the general formula of $A_2M(I)M(III)X_6$, whose crystal structure is shown in Figure 2a. The alternating $[M(I)X_6]^{5-}$ and $[M(III)X_6]^{3-}$ octahedra are connected by the X halogens, remaining its 3D structure. Another strategy is to replace two $[PbX_6]^{4-}$ with a $[M(IV)X_6]^{2-}$ and a $[VX_6]^{6-}$ octahedron where V is a vacancy, thus forming a vacancy-ordered double perovskite. Therefore, the lead-free double perovskite has a rich structural and functional diversity by combining different A, M, and X elements. It should be noted that not all metal ions can replace Pb^{2+} to form stable double perovskite. Generally, to assess the structural stability of perovskite, the octahedral factors **μ** and tolerance factors **τ** with high prediction accuracy are proposed as:

$$\tau = \frac{r_x}{r_B} - n_A\left\{n_A - \frac{r_A/r_B}{\ln(r_A/r_B)}\right\} \tag{1}$$

$$\mu = \frac{r_B}{r_x} \tag{2}$$

where r_A, r_B, and r_X represent the ionic radius of different ions and n_A is the oxidation state of A. For double perovskite, the r_B is the average radius of the two heterovalent metal cations. When τ is smaller than 4.18 and μ is between 0.44 and 0.90, we can predict that the perovskite structure is stable. In addition to the above factors, the decomposition energy is also very important and should be considered to design stable lead-free double perovskite. Although hundreds of double perovskites have been calculated to be thermodynamically stable, a limited part of them was experimentally synthesized and investigated. We summarise the synthesized stable lead-free double perovskite in Figure 2b and we review their applications as perovskite photodetectors in the following section.

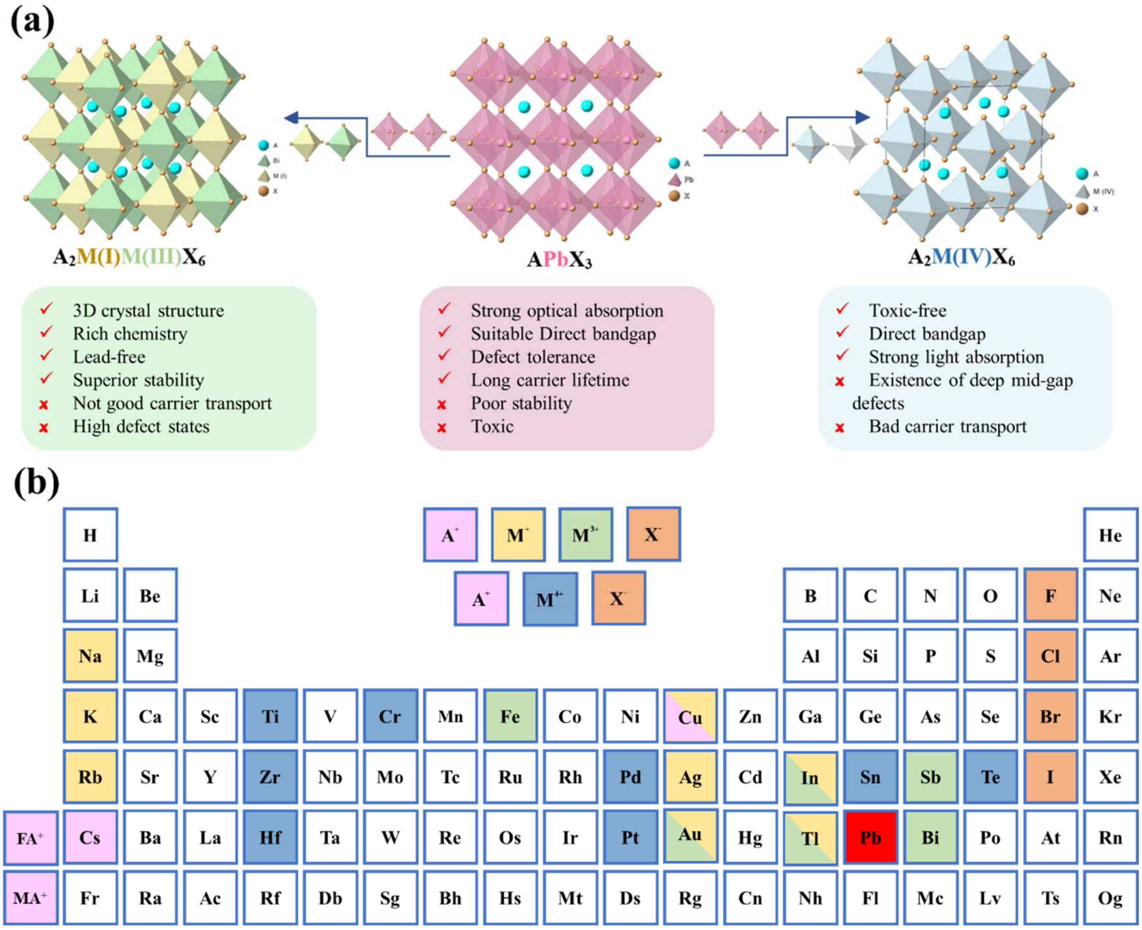

Figure 2. (a) The structure evolution from lead-based perovskite to lead-free double perovskite and their pros and cons. (b) Summary of the synthesized lead-free double perovskite materials.

4. $A_2M(Ⅰ)M(Ⅲ)X_6$-based double perovskite photodetector

The quaternary double perovskites with $A_2M(I)M(III)X_6$ structure, such as $Cs_2AgBiBr_6$[3], $Cs_2AgInCl_6$[4], and $Cs_2AgSbCl_6$[5], have been extensively studied recently due to their notable advantages of high inherent chemical stability, low toxicity, and long carrier lifetime. In this section, we review the basic optoelectrical performance of photodetectors by categorizing them as Bi-based, Sb-based, In-based, Fe-based, Tl-based, and Au-based double perovskite.

4.1. Bi-based double perovskite photodetector

Among the $A_2M(I)M(III)X_6$ materials, Bi^{3+}, which has a similar electronic configuration ($6s^26p^0$), electronegativity, and ionic radius with Pb^{2+}, is considered to be the most promising candidate to replace the Pb^{2+} ion.[6] Bi-based double perovskite such as $Cs_2AgBiBr_6$, $Cs_2AgBiCl_6$, Cs_2AgBiI_6 (nanocrystals), $MA_2AgBiBr_6$, $Cs_2NaBiCl_6$, MA_2KBiCl_6, $Cs_2LiBiCl_6$, etc, has been widely studied in photovoltaic and photodetector fields due to its high optical absorption coefficient, and long carrier recombination lifetime. Among them, $Cs_2AgBiBr_6$[7] stands out because of its small carrier effective mass, high humidity, and heat stability.

In 2018, the double perovskite $Cs_2AgBiBr_6$ film was first used in photoconductive photodetectors, presenting a high responsivity of 7.01 A W^{-1}, a specific detection rate of 5.66×10^{11} Jones, an on/off photocurrent ratio of 2.16×10^4, and a fast response rate of 956/995 μs[8]. This work provides prospects for the development of $Cs_2AgBiBr_6$ lead-free perovskite in photoelectric detection applications. To manufacture $Cs_2AgBiBr_6$ photodetectors with a wider response range, higher responsivity, and higher detection rate, it is necessary to carefully tune its bandgap, and optimize the interface between ETL/HTL and the perovskite absorber layer. For example, in 2020, to improve the quality of $Cs_2AgBiBr_6$ double perovskite film, Mai et al.[9] fabricated $Cs_2AgBiBr_6$ film on substrates coated with ultra-thin metal oxide (MO_x) layer, and used it as weak light photodetectors with the FTO/ALD-MO_x

interlayer/$Cs_2AgBiBr_6$/ETL/Au structure. Figure 3a describes the schematic diagram of Bi-O bond formation at the interface between the ALD-Al_2O_3 modified substrate and $Cs_2AgBiBr_6$ film. Compared with bare devices of photodetectors, the switching ratio is increased by 10 times, and the minimum detection radiation is reduced from 9.7×10^{-8} W cm^{-2} to 1.9×10^{-9} W cm^{-2} (Figure 3b, 3c), and the detection rate is improved from 3.3×10^{11} jones to 1.2×10^{13} jones (Figure 3b, 3c). This is because the Bi-O (or Ag-O) bond formed between the MO_x substrate and the perovskite interface contributes to the improvement of the quality of the $Cs_2AgBiBr_6$ film, resulting in films with large grain size and reduced pinholes. It is also known that proper ETL and HTL can help to optimize the perovskite morphologies and greatly improve the photocarrier transport efficiency, which is conducive to realizing high-performance photodetectors. Benefiting from the intrinsic p-type semiconductor nature and the satisfying properties of adequate energy levels, high hole mobility（1.2×10^{-3} cm^2 V^{-1} s^{-1}）, and good thermal stability, inorganic copper thiocyanate (CuSCN) has attracted widespread attention for applying on perovskite-based devices as a hole transport layer[10-12]. Inorganic thiocyanate (CuSCN) was introduced to work as the hole transport layer (HTL) for a self-powered $Cs_2AgBiBr_6$ photodetector in 2020[13]. The device structure is shown in Figure 3d. Compared with devices without a CuSCN hole transport layer, the light detection limit is reduced from ~7×10^{-9} W cm^{-2} to 1×10^{-9} W cm^{-2}, which facilitates its usage for weak light imaging. The specific detection rate was increased from 1.74×10^{12} Jones to 1.03×10^{13} Jones and the responsivity was increased from 0.04 A W^{-1} to 0.34 A W^{-1}, which was because the CuSCN hole transport layer can improve the device carrier separation and collect efficiency. Under ideal conditions, the $Cs_2AgBiBr_6$ absorbs photo energy to generate carriers. The built-in electric field separates the carriers into electrons and holes. The electrons flow to the FTO layer, and the holes move to the Au electrode, which minimizes the recombination of carriers and generates the effective output of electrical signals. However, as illustrated in Figure 3e, since the work function of the Au electrode is located between the top of the valence band and the bottom of the conduction band of $Cs_2AgBiBr_6$, both electrons and holes will flow to the Au electrode and cause the energy losses. After introducing the CuSCN hole layer, the electron pathways to Au are blocked and holes can be collected more efficiently, thus the performance of the device is greatly improved.

As for the ETLs, in 2022, Shen et al.[14] introduced ZnO/SnO_2 double ETL into $Cs_2AgBiBr_6$ double perovskite-based photodetectors. Compared with the detectors with single ZnO ETL, the response rate and specific detection rate of the detector at 450 nm with the SnO_2/ZnO double ETL are 12.7 times and 16.5 times higher, respectively. The significant improvement in device performance is attributed to the introduction of SnO_2, which solves the mismatched energy levels problem between the ZnO ETL and perovskite film[15,16], reduces the energy loss at the interface, and optimizes electron transport and extraction. Meanwhile, the hydrophobic surface property of ZnO usually leads to a poor perovskite film [17, 18]. After inserting the SnO_2/ZnO double ETL, the interface has good wet stability, allowing for the formation of smooth and pinhole-free perovskite films[19, 20]. Interestingly, ultraviolet immersion is also an effective strategy to improve photodetection performance. In 2022, Yuan and coworkers[21] performed UV immersion treatment on several $Cs_2AgBiBr_6$-based photodetectors with different structures. The results showed that UV treatment increased the photocurrent (from ~ 1.0×10^{-5} A to ~ 1.5×10^{-4} A) and response speed (from 30.1 μs to 340 ns). To further investigate the potential mechanism responsible for this phenomenon, space charge-limited current (SCLC) tests were performed, and the results showed that the defect density of the untreated and UV-treated devices was 8.97×10^{16} and 3.33×10^{16} cm^{-3}, respectively. This finding demonstrates that continuous UV illumination can passivate the perovskite body and interface defects[22-26], increase the carrier concentration and/or mobility， and thus achieve the purpose of enhancing the performance of perovskite detector devices. These results drive the development of double perovskite-based photodetectors.

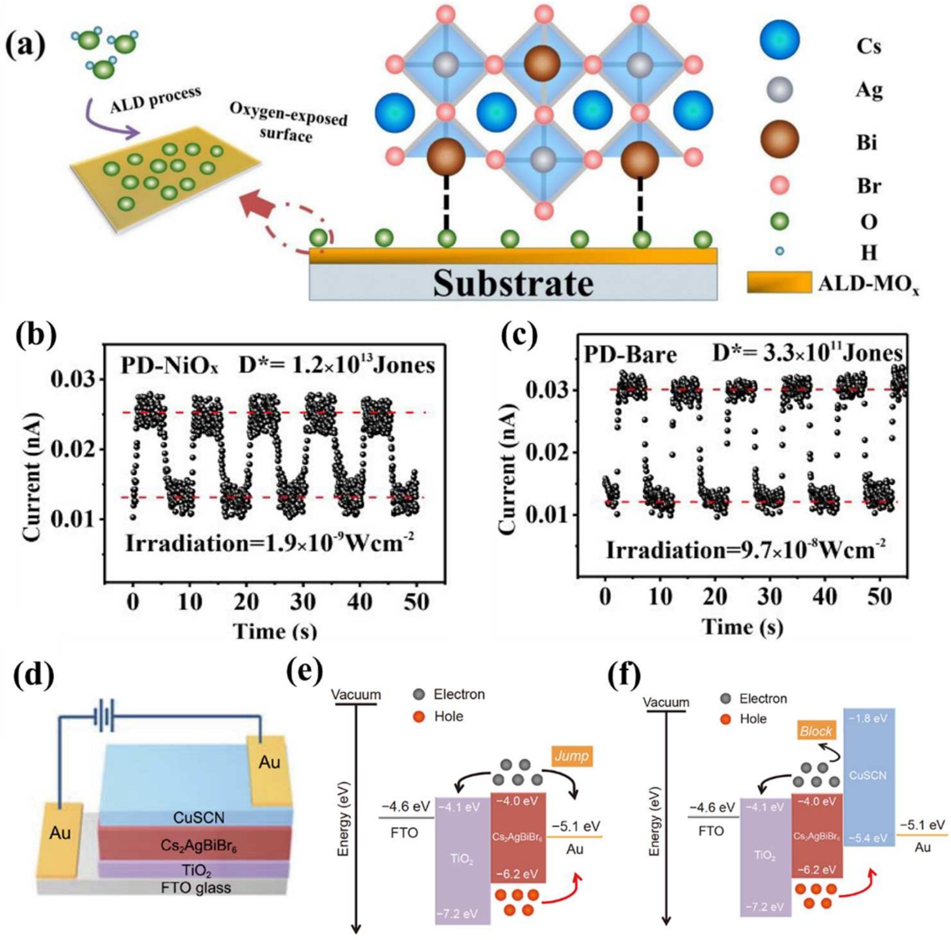

Figure 3. (a) Schematic diagram of the Bi-O interfacial interaction at ALD-MO_x layer modified substrate/$Cs_2AgBiBr_6$ interface.[9] Copyright 2020, American Chemical Society. Typical photoresponse curves of (b) PD-NiO_x PD and (c) PD-Bare PD under their minimum detected irradiations.[9] Copyright 2020, American Chemical Society. (d) Schematic of the $Cs_2AgBiBr_6$-based PD.[13] Copyright 2020, Science China Press and Springer. Energy-band diagrams of the devices (e) with and (f) without CuSCN HTL[13]. Copyright 2020, Science China Press and Springer.

In addition, $Cs_2AgBiBr_6$ also has promising applications in X-ray detectors[27]. Depending on the detection principle, X-ray detectors can be divided into direct and indirect detectors. The principle of indirect X-ray detectors is to use scintillators to convert X-rays into visible light, and then use photodiodes to convert them into electrical signals and record them[28, 29], which has the advantages of low cost and stable performance[30, 31]. But in the photoelectric conversion process, X-ray photons need to undergo two energy conversion processes, resulting in increased energy loss. Besides, the detection sensitivity and spatial resolution are affected due to optical crosstalk during scintillation[32]. Direct-type detectors use semiconductors to convert X-ray photoelectrons directly into electronic signals, which makes the detection signal easier and faster collected and then the signal reproducibility is better[33]. Therefore, direct X-ray detectors have the advantages of high sensitivity, high energy resolution, and better spatial resolution for X-ray imaging. Currently, direct X-ray detectors based on perovskite are still in their infancy. According to $\alpha \propto Z^4/E^3$, the higher the average atomic number (Z), the higher the X-ray attenuation coefficient (α) and the higher the light absorption efficiency. $Cs_2AgBiBr_6$ has a large average atomic number (Cs 55, Ag 47, Bi 83)， high density (4.65 g cm^{-3}), and high resistivity, with superior photoelectric properties such as sensitivity and detection limit compared to traditional materials. These characteristics make $Cs_2AgBiBr_6$ have commercial prospects in the field of X-ray detection. Currently, the X-ray detector based on $Cs_2AgBiBr_6$ has made great progress[34]. Tang's group[35] reported an X-ray detector based on $Cs_2AgBiBr_6$ single crystals for the first time. The device achieved a low detection limit of 59.7 nGy_{air} s^{-1} by passivating the bulk phase and surface defects of $Cs_2AgBiBr_6$ single crystals by thermal annealing and surface treatment. Subsequently, Julian et al.[36] studied the electronic properties of

$Cs_2AgBiBr_6$ at room temperature and liquid nitrogen temperature. It is found that lowering the temperature from room temperature to liquid nitrogen temperature can increase the carrier lifetime and resistivity of $Cs_2AgBiBr_6$ perovskite, which led to an increase in detector sensitivity from 316 μC $Gy_{air}^{-1}cm^{-2}$ to 988 μC $Gy_{air}^{-1}cm^{-2}$. Although low-temperature technology requires high experimental conditions, this result provides ideas on how to improve the detector sensitivity. In addition, Shao et al.[37] synthesized $Cs_2AgBiBr_{5.933}Cl_{0.067}$ SC by doping Cl ions in $Cs_2AgBiBr_6$, which exhibited low trap density of states and high carrier mobility. It achieved excellent device performance in X-ray detection, including a superior X-ray detection sensitivity of 714 μC $Gy_{air}^{-1}cm^{-2}$, and a minimum dose rate as low as 36.48 $nGy_{air}\ s^{-1}$. Currently, achieving long-term operational stability is the future research direction of $Cs_2AgBiBr_6$-based double perovskite X-ray detectors[38]. $Cs_2AgBiBr_6$ is prone to defect formation, such as anti-situ defects (AgBi or BiAg) and vacancy defects (Bi or Br vacancies)[39], which severely limits the preparation of X-ray detectors with lower detection limits and higher sensitivity, as well as the operational reliability of devices. Considering these parameters, further research on X-ray detectors based on $Cs_2AgBiBr_6$ is needed.

4.2. Other (Sb^{3+}, Fe^{3+}, In^{3+}, Tl^{3+}, Au^{3+}-based) double perovskite photodetector

Apart from the Bi^{3+} ion, Sb^{3+} ($5s^25p^0$) ion also has similar electronic structures to the Pb^{2+} ion. Theoretically, it can be used as a candidate to replace the Pb^{2+} ion. At present, $Cs_2AgSbBr_6$[40] (band gap of 1.64 eV) and $Cs_2AgSbCl_6$[41] (band gap of 2.54 eV) have been successfully synthesized. Currently, there is no report on Cs_2AgSbX_6-based photodetector and this is because of the high formation energy of Cs_2AgSbX_6 and the small ionic radius of Sb^{3+}. These crystals are accompanied by large amounts of secondary phases such as $Cs_3Sb_2Br_9$ and Cs_2AgBr_3 and unreacted AgBr[42]. Moreover, based on Ag/Sb ion，$(4,4\text{-DFPD})_4AgSbI_8$ (4,4-DFPD=4,4-difluoropolipiridium) 2D iodide perovskite has been successfully applied in X-ray detection, which possesses promising X-ray responsivity with a sensitivity as high as 704.8 μC Gy_{air}^{-1} cm^{-2} at 100 V bias and a detection limit as low as 0.36 μGy_{air} s^{-1} at 10 V bias[43]. In recent years, Fe-based double perovskites such as $Cs_2AgFeCl_6$ and $Cs_2NaFeCl_6$ has attracted increasing attention with their excellent optical absorption property[44]. Unfortunately, even at low temperatures, there is no detectable PL in the $Cs_2AgFeCl_6$ or $Cs_2NaFeCl_6$ crystal which would limit its application in optoelectronic fields. As a member of the $A_2M(I)M(III)X_6$ double perovskite family, $Cs_2AgInCl_6$ has a large direct band gap (3.2 eV), which determines that $Cs_2AgInCl_6$ mainly absorbs light with a wavelength less than 400 nm, so it can be used to manufacture ultraviolet photodetectors[45]. Tang and coworkers designed and manufactured a photoconductive planar ultraviolet detector based on $Cs_2AgInCl_6$ single crystal[46], which showed a current switching ratio of ~ 500, a light response speed of ~ 1 ms, a low dark current (~ 10 pA at 5 V bias), and a high detection rate (~ 10^{12} Jones). The $Cs_2AgInCl_6$ single crystal shows two absorption edges at 384 and 595 nm respectively, corresponding to inter-band transition (from CBM to VBM-2) and parity-induced forbidden transition (from CBM to VBM). The parity-forbidden transition in the direct band gap system leads to very weak emission of $Cs_2AgInCl_6$, which hinders its practical application in optoelectronics. Alloying or doping in $Cs_2AgInCl_6$ can break the parity forbidden transition, change the band gap, improve the luminous efficiency, and ultimately improve the detection performance. At present, the doping of transition metal ions such as Cu^{2+}[47], Mn^{2+}[48], and lanthanide elements has been explored. In 2022, Qiu and coworkers[49] synthesized $Cs_2Na_xAg_{1-x}InCl_6$ (X=0.16, 0.4, 0.58, 0.78, 1) nanocrystals with different amounts of sodium doping by hydrothermal method. The introduction of Na^+ improved the photoluminescence intensity of $Cs_2AgInCl_6$, where x=0.78 has the highest luminous intensity. The broadband emission range of the sample is 400 ~ 800 nm, covering the whole visible spectrum. The transparent composite film prepared based on $Cs_2Na_{0.78}Ag_{0.22}InCl_6$ crystals mixed with PMMA can capture weak solar blind near-ultraviolet light, convert it to visible light, and display the captured signal on a digital oscilloscope after being sensed by a light correlation resistor (LDR). The device has a response speed of about 0.5 s and has high detection stability. Tl^{3+}, which is in the same main group as In^{3+}, can also be used as the M-site ion of $A_2M(I)M(III)X_6$ double perovskite. In 2018, Karunadasa and coworkers synthesized for the first time double perovskite $Cs_2AgTlCl_6$ and $Cs_2AgTlBr_6$ based on Tl by slow cooling crystallization method. Both of them have a cubic double perovskite structure with $Fm\overline{3}m$ symmetry at room temperature. $Cs_2AgTlBr_6$ possesses the smallest reported direct band gap for a halide perovskite at 0.95 eV. Meanwhile, $Cs_2AgTlBr_6$ and $Cs_2AgTlCl_6$ have good environmental stability, with no change in their XRD peak position when exposed to light

(0.75 suns, 60°C) or humid air (55% relative humidity) for 40 days. Preliminary results show that Cs_2AgTlX_6 has the potential to convert light into electricity[50]. However, Tl is highly toxic and this would hinder its future development. In addition to the above double perovskite, gold-based double perovskite has attracted researchers' attention due to its narrow direct band gap (1.06 eV)[51]. In the gold-based double perovskite structure, gold and halogen ions form a compressed octahedron $[Au^+X_6]^{5-}$ and elongated $[Au^{3+}X_6]^{3-}$ octahedrons, respectively. The two octahedrons form a tetragonal $Cs_2Au_2X_6$ through the shared connection of halogen ions. The electronic band structure shows that $Cs_2Au_2X_6$ has a slight indirect band gap, and the difference between the indirect band gap and the optically permissible direct band gap is very small, only about 0.03 eV[52]. Like Fe-based double perovskite, $Cs_2Au_2I_6$ also has no detectable PL, and the cause of this phenomenon remains to be investigated. Preliminary results have demonstrated that gold-based double perovskite can convert light into electricity and deliver a solar-to-electricity efficiency for $MA_2Au_2I_6$[53].

5. $A_2M(IV)X_6$-based double perovskite photodetector

Since Sn^{4+} single crystals were first reported in 2013, an increasing number of novel $A_2M(IV)X_6$ double perovskite with exciting optoelectronic properties has emerged[54]. There are high hopes for the great potential of vacancy-ordered $A_2M(IV)X_6$ in various photoelectric applications. In this section, we discuss the fundamental properties of double perovskite with $A_2M(IV)X_6$ structure and its recent progress in the field of photodetectors.

5.1. Sn-based double perovskite photodetector

Among all bivalent substitution elements for Pb^{2+}, Sn^{2+} is considered one of the most promising candidates due to its similar electronic structure and ionic radius (1.35 Å for Sn^{2+} and 1.49 Å for Pb^{2+}) with Pb^{2+}. However, the 5s orbitals in Sn^{2+} cations are susceptible to oxidation and will generate a large density of oxygen vacancies, thus limiting the charge transport and even leading to material degradation[55]. Therefore, Sn^{2+}-based perovskite is extremely unstable in the ambient atmosphere. In contrast, the Sn^{4+} ion exhibits excellent stability to moisture and light due to the filled $4d^{10}$ electron orbitals and high electronegativity. Recently, vacancy-ordered double perovskites A_2SnX_6, which have direct band gaps, adjustable light response range, and high air and moisture stability, have attracted increasing attention in optoelectronic detection applications.

Han et al[56] synthesized lead-free double perovskite Cs_2SnX_6 (X = I and Br) with high crystallinity and high yield by a hydrothermal method in 2019 and fabricated a double-ended photodetector with a simple structure of FTO/Cs_2SnI_6/FTO to explore the potential applications of Cs_2SnI_6 for photodetection. As shown in Figure 4a, the Cs_2SnI_6 film will generate free carriers under appropriate light irradiation, and then the carriers are collected by the opposite electrodes with the help of the external electric field, thus producing an efficient photoresponse current. The current-time (I-T) response of the Cs_2SnI_6 photodetector was tested under intermittent irradiation and 3V bias. The results showed that the rise time (t_r) and decay time (t_d) of the Cs_2SnI_6 photodetector were less than 100 ms. More importantly, the unencapsulated Cs_2SnI_6 photodetector shows superior stability to moisture and light because of the stable crystal structure and chemical composition of Cs_2SnI_6.

To realize high-performance photodetectors, it is vital to fabricate high-quality pure-phase Cs_2SnI_6. So far, the main methods for preparing Cs_2SnI_6 thin films are vapor deposition and solution deposition[57]. The evaporation method has strict requirements for reaction conditions and precursors, which usually needs high temperature, high vacuum, and long reaction time. Besides, the SnI_4 will be thermally decomposed during thermal evaporation. In contrast, the one-step spin-coating is an efficient and low-cost method for preparing Cs_2SnI_6 films. However, the solution-deposited films usually present imperfect morphologies with pinholes, impurities, and low film coverage which is believed to be caused by the too-slow nucleation and crystallization. Therefore, optimizing the reaction conditions and preparing high-quality Cs_2SnI_6 films or crystals is the first task to achieve high-performance photodetectors. Krishnaiah et al.[58] optimized the preparation process of Cs_2SnI_6 thin film. It was found that at a specific environmental condition, i.e., the relative humidity is less than 40% and the annealing temperature is kept at 75℃, the Cs_2SnI_6 perovskite thin film becomes pure and dense. In all other conditions with higher RH% (50%, 60%, 80%) and annealing temperature, the impurity CsI phase is detected together with the Cs_2SnI_6 phase for the fabricated films. At 1 V bias voltage, the maximum R_{ph} and D_{ph} for Cs_2SnI_6 PD were 6 mA W^{-1} and 2.00×10^9 Jones, respectively. To

Preprints (www.preprints.org) | NOT PEER-REVIEWED | Posted: 28 April 2023 doi:10.20944/preprints202304.1145.v1

further improve the performance of the Cs_2SnI_6 detector, Tan and coworkers[59] innovatively developed a precursor compensation treatment (PCT) technique by spin-coating SnI_4/isopropanol solution on the as-prepared Cs_2SnI_6 film, which provides an I-rich environment for the growth of the Cs_2SnI_6 film, compensating for the SnI_4 loss and suppressing the formation of inherent defects. As shown in Figure 4b and Figure 4c, the Cs_2SnI_6-PTC films were dense and smooth with fewer defects and higher coverage compared to the unoptimized films. Photodetectors with a configuration of FTO/c-TiO_2/Cs_2SnI_6/spiro OMeTAD/Au were fabricated. Under zero bias and light illumination with different intensities, the maximum response of PCT-Cs_2SnI_6 PD reaches 1.07 mA W^{-1}, and the specific detection rate is 6.03×10^{10} Jones. Both of which are higher than the control group (R=0.0059 mA W^{-1}, D*=2.94×10^{10} Jones), suggesting that the ability to detect white light and weak light signals was enhanced. Moreover, compared with the control group, the PCT-Cs_2SnI_6 PD exhibited a higher switching ratio (Figure 4d) and faster response speed (Figure 4e). It is noted that surface defects in double perovskite are a cause of its reduced resistance and increased dark current, which also affects the performance of detector devices. Very recently, Shen and his colleagues[60] reported that introducing metal ions of Zn^{2+} and Ni^{2+} into Cs_2SnI_6 can reduce the surface defects of perovskite. The Cs_2SnI_6 nanochip detector based on metal ion doping shows a spectral response at 400 - 900 nm. Specifically, the Cs_2SnI_6 device doped with Ni^{2+} has an excellent response rate of 1.6×10^3 A W^{-1}, and the Cs_2SnI_6 device doped with Zn^{2+} has a high detection rate of 1.56×10^{13} Jones (Figure 4f). The performance of Cs_2SnI_6 device based on metal ion doping exceeds that of other lead-free perovskite-based photodetectors, and even reaches the level of the best reported lead-based perovskite photodetectors. This is inspiring for the research and development of lead-free double perovskite-based photodetectors.

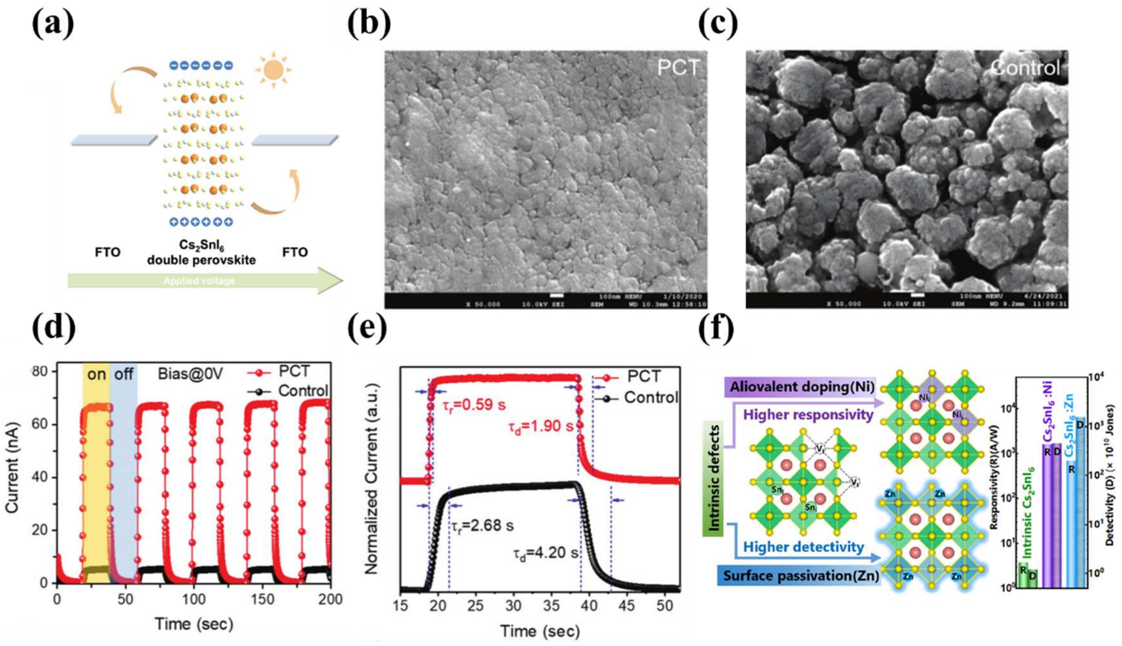

Figure 4. Cs_2SnI_6-based photodetectors. (a) Schematic working mechanism.[56] Copyright 2019, Wiley. SEM images of the PCT-Cs_2SnI_6 film (b) and control sample(c).[59] Copyright 2021, Royal Society of Chemistry. (d) Photo-switching characteristics of the PCT-Cs_2SnI_6 PD and control device at zero bias with the periodic illumination.[59] Copyright 2021, Royal Society of Chemistry. (e) Rising and falling edges of one response cycle for determining the response time of the Cs_2SnI_6 PDs.[59] Copyright 2021, Royal Society of Chemistry. (f) A schematic diagram of the crystal structure of Cs_2SnI_6 perovskites with Zn ion and Ni ion incorporation.[60] Copyright 2023, American Chemical Society.

5.2. Other (Ti^{4+}, Pd^{4+}, Hf^{4+}, Te^{4+}, Cr^{4+}, Zr^{4+}-based) double perovskite photodetector

Since many transition metals have stable +4 oxidation states, meanwhile, they are non-toxic or low toxicity, researchers have explored the possibility of replacing Sn^{4+} in Cs_2SnI_6 with appropriate transition metal cations. Among them, Ti^{4+}, Pd^{4+}, Hf^{4+}, Te^{4+}, Cr^{4+}, and Zr^{4+} have been proven to be thermodynamically stable and have been synthesized.

In 2022, Ye and colleagues[61] screened 10 covalent substituents of M-site metal ions in vacancy-ordered double perovskite $Cs_2M(IV)X_6$ using the density functional theory (DFT). Among them, for Ti, Zr, and Hf elements in the same group, the band gap (0.86 eV, 1.8 eV, 2.2 eV (X=I)) increased with the increase of the M-site cation radius. The transition from chloride to bromide and then to iodide gradually narrows the band gap, as shown in Figure 5a. Ti-based double perovskite is non-toxic, earth-abundant, and biocompatible. DFT calculation shows that the band gap of Cs_2TiX_6 material is between 1.5 and 2.96 eV, and has a large absorption coefficient in the visible light range. In detail, the maximum absorption coefficient of Cs_2TiBr_6 at 422 nm is about 3×10^5 cm^{-1}, the absorption coefficient of Cs_2TiI_6 at 526 nm is 2.35×10^5 cm^{-1}, and the absorption coefficient of Cs_2TiCl_6 at 380 nm is 2.22×10^5 cm^{-1}. Besides, Ti-based double perovskite has high optical conductivity (10^3 Ω^{-1} cm^{-1}) and a good refractive index in the visible range. These optical properties make it promising for optoelectronic applications[62]. For instance, the Cs_2TiBr_6 solar cell has been demonstrated with a photo-to-electric conversion efficiency of 3.3%[63]. Its corresponding photo-detecting application is still waiting to be verified. The A_2TeX_6 compound (A=MA, FA, or BA; X=Br^- or I^-; MA=CH_3NH_3; FA=$CH(NH_2)_2$; BA=benzylamine), as a member of the vacancy-ordered double perovskite, has also attracted the attention of researchers. It has an adjustable band gap (1.42-2.02 eV), high mobility (~65 cm^2 V^{-1} s^{-1}), long carrier diffusion length (38 μm), and good thermal stability. [64] The single-crystal XRD patterns indicate that the crystal structure of both MA_2TeI_6 and MA_2TeI_6 belongs to the cubic $Fm\bar{3}m$ space group. [65] Their crystal structures are shown in Figure 5b.[64] Guo and coworkers[66] prepared Cs_2TeI_6 films on flexible polyimide (PI) substrates by electrospray and used them in X-ray detectors. The device structures are shown in Figure 5c, which are PI/Cs_2TeI_6/Au and glass/FTO/TiO_2/Cs_2TeI_6/Au, respectively. The flexible and rigid devices show a high sensitivity of 59.28 and 76.27 μC Gy_{air}^{-1} cm^{-2} at 5 V bias voltage and 20 kV X-ray, respectively. Cs_2CrI_6, as a new vacancy-ordered perovskite, possesses more excellent stability and optical absorption, suitable band gap (1.08 eV), higher mobility (~10^3 cm^2/V), and lower capture cross-section compared to the $MAPbI_3$[67]. Based on the first-principle calculations, the calculated electron and hole mobilities of Cs_2CrI_6 (μ_n=7.24×10^3 cm^2/V, μ_p=6.57×10^3 cm^2/V) are larger than those of $MAPbI_3$ (μ_n =24.8 cm^2/V, μ_p =293 cm^2/V)[68,69]. The superior mobility suggests that Cs_2CrI_6 may possess greater potential than $MAPbI_3$ in the application of photodetectors. We note that many novel lead-free double perovskite materials emerge and have been utilized in photoelectric applications. We therefore summarize the device structures and the corresponding performances of the photodetectors involved in this paper in Table 1 for a better comparison.

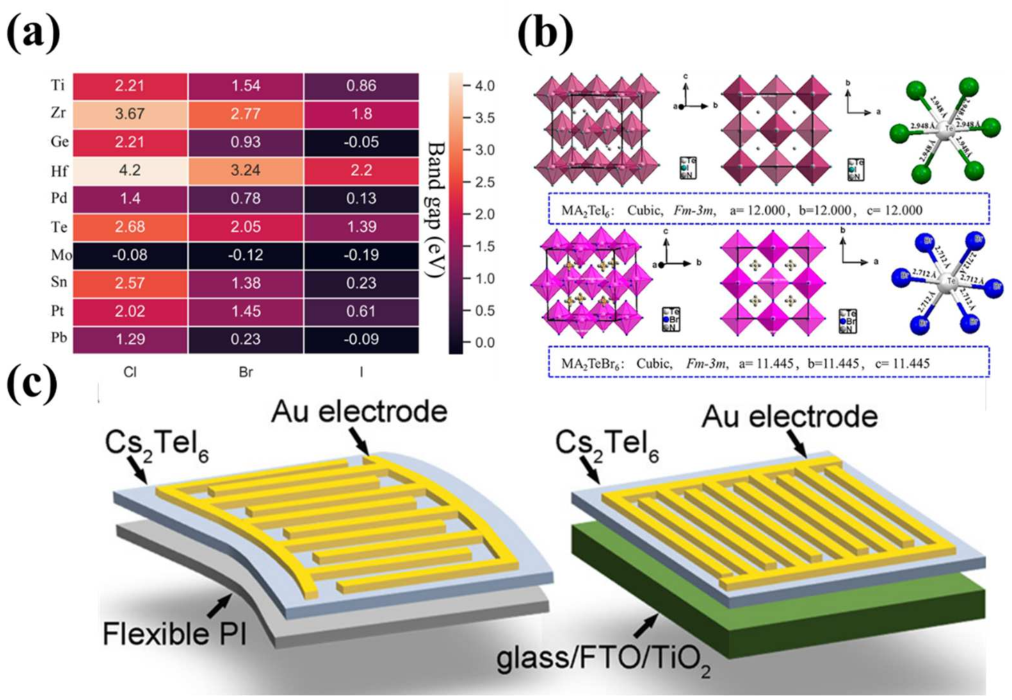

Figure 5. (a) Results of bandgap prescreening of the studied 30 perovskites.[61] Copyright 2022, Wiley. (b) The crystal structures of MA_2TeI_6 and MA_2TeBr_6.[64] Copyright 2019, American Chemical Society. (c) Sketches of

Cs_2TeI_6 detector structures based on the flexible PI and rigid FTO substrates.[66] Copyright 2021, American Chemical Society.

Table 1. Summary of key parameters of photodetectors based on lead-free double perovskite.

Device configuration	Spectral range (nm)	R（A W^{-1}）	D^* (jones)	Response time (ms)	On/off ratio	Ref.
$Au/Cs_2AgBiBr_6/Au$	300-800	7.01	5.66×10^{11}	0.956/0.955	2.2×10^{4}	8
ALD-NiOx modified $FTO/Cs_2AgBiBr_6/TiO_2/Au$	350-550	-	1.2×10^{13}	-	-	9
$FTO/TiO_2/Cs_2AgBiBr_6/CuSCN/Au$	300-600	0.34	1.03×10^{13}	28.75/32.95	-	10
$FTO/SnO_2/ZnO/Cs_2AgBiBr_6/Au$	-	0.608	2.97×10^{10}	124/61	-	14
$FTO/Cs_2AgBiBr_6/Au$	350-500	9.8	-	$1.2\times10^{-3}/0.5\times10^{-3}$	-	21
$Au/Cs_2AgInCl_6/Au$	340–400	0.97	$\sim10^{12}$	0.8/1.0	~500	46
$FTO/Cs_2SnI_6/FTO$	-	0.006	2×10^{9}	-	-	56
$FTO/c\text{-}TiO_2/Cs_2SnI_6/Spiro\ OMeTAD/Au$	300-1000	0.001	6.03×10^{10}	590/190	151	59
$FTO/TiO_2/Cs_2SnI_6\text{-}Ni^{3+}/TiO_2/FTO$	350-950	160	4.52×10^{12}	-	-	60
$FTO/TiO_2/Cs_2SnI_6\text{-}Zn^{2+}/TiO_2/FTO$	350–900	710	1.56×10^{13}	190/530	-	60
$Au/(4FPEA)_4AgBiI_8/Au$	400	0.002	5×10^{8}	-	-	70
$Au/(4FPEA)_4AgBiI_8/Au$	400	0.01	6×10^{9}	-	-	70
$ITO/Cs_2AgBiBr_6/SnO_2/Au$	350	0.11	2.1×10^{10}	2	-	71
$SnO_2/Cs_2AgBiBr_6/TFB/Au$	300-550	0.14	3.3×10^{12}	1.7×10^{-5}	-	72
$FTO/Cs_2SnI_6/FTO$	500–900	-	-	100/100	-	73
$MWCNT/Cs_2SnCl_6{:}Bi/GaN$	350–400	0.208	1.2×10^{12}	$7.5\times10^{-4}/9.1\times10^{-4}$	-	74
$In/GaN/Cs_2AgBiBr_6/Ag$	200–550	1.46	9.4×10^{12}	3.463/8.442	-	75
$Au/Cs_2AgBiBr_6$ microplatelets/Au	450	0.245	1.3×10^{11}	$145\times10^{-3}/136\times10^{-3}$	2.8×10^{3}	76
$Au/MA_2AgBiBr_6$ microplatelets/Au	450	0.058	2.9×10^{10}	-	281	76
$ITO/Cs_2PdBr_6/Ag$	-	-	-	-	-	77
Flexible $ITO/SnO_2/Cs_2AgBiBr_6/Carbon$	-	0.031	8.04×10^{11}	-	0.5×10^{4}	78

ITO/$Cs_2AgBiBr_6$/Ag	375	-	-	$6.13\times10^{-3}/28.02\times10^{-3}$	6.6×10^{3}	79

6. Challenges and Perspective for Lead-Free Double Perovskite-based PDs

As mentioned in the previous section, lead-free double perovskite photodetectors have received a lot of research attention in recent years and have achieved impressive progress. Despite the tremendous progress in photodetection, there are still many challenges in the future direction of this field, which may hinder the development of lead-free double perovskite and limit its potential applications. To fabricate higher-performance photodetectors, we systematically summarized the challenges faced by various types of lead-free double perovskite for photodetectors and proposed the corresponding solutions, as summarized in Figure 6 and discussed as follows:

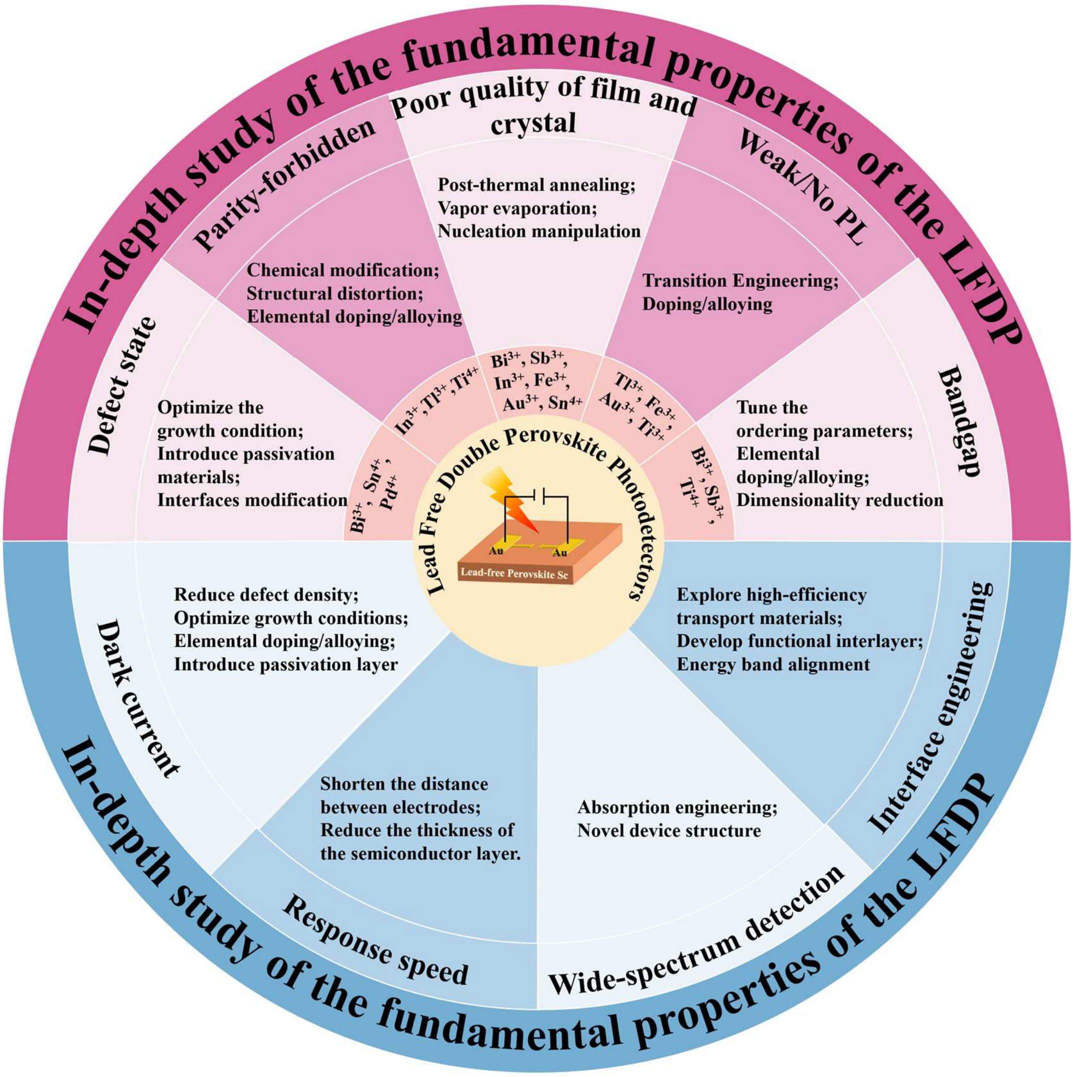

Figure 6. Summary of the challenges and viable strategies of the lead-free double perovskite photodetectors.

(1)In-depth understanding of the fundamental material properties of the lead-free double perovskite is needed. Compared with the well-studied lead-based perovskite, lead-free double perovskite, as a new branch of perovskite materials, is undoubtedly underinvested and many aspects have not been effectively and deeply investigated. To explore the potential of lead-free double perovskite, researchers need to investigate more deeply its potential mechanism, crystal structure, and optoelectronic properties.

We summarized five material challenges that limit the wide application of double perovskite in optoelectronics. First, compared to the conventional lead-based perovskite, double perovskite has more deep-level defect states in the lattice and bulk phases, which leads to reduced its carrier mobility and lifetime. To understand the mechanism of defect traps in the structure, the basic charge carrier dynamics need to be studied in detail. The growth condition need to be carefully tuned to obtain high-qulity perovskite absorber. Meanwhile, the methods of defect passivation and surface modification of lead-free perovskite should be explored. For example, the incorporation of non-volatile Lewis-base molecules such as urea and thiourea into the perovskite precursor solution can regulate crystal growth and cause single crystals to precipitate along grain boundaries to passivate defects[80].

Second, for some lead-free double perovskites with indirect bandgap, such as Bi-based, Sb-based, and Ti-based, they require phonon emission or absorption to maintain momentum, which lead to their relatively low absorption coefficients[81]. Bandgap engineering can modulate the optoelectronic properties of lead-free double perovskite to make the transition from indirect bandgap to direct bandgap. The engineering strategy mainly consists of elemental doping/alloying and tuning the ordering parameters. Doping and alloying are the most powerful methods for adjusting the optical, electrical, and structural properties of perovskite.[82] For example, through alloying with In^{3+} or Sb^{3+}, the indirect bandgap of bulk $Cs_2AgBiBr_6$ (2.12 eV) has been altered to 2.27 and 1.86 eV, respectively, which is caused by the different atomic configurations of In and Sb. However, most of the In and Sb alloyed samples show reduced PL intensity, suggesting the presence of relatively deep defect states. The ordered-disorder parameters can be intentionally adjusted through growth regulation or external pressure treatment, resuting the changes in the bandgap.[82] Direct bandgaps can be also achieved from some low-dimension structures such as the $(BA)_4AgBiBr_8$[83] and $(AE2T)_2AgBiI_8$[84].

Third, for double perovskite compounds with direct but parity-forbidden transition gaps, such as $Cs_2AgInCl_6$, $Cs_2AgTlCl_6$, $Cs_2NaInCl_6$, Cs_2TiBr_6, they have poor absorption ability for photons with energies close to the bandgap. Chemical modification, structural distortion or elemental doping can be used to eliminate or break the optical transition selection rules and make them more suitable for photoelectrical applications. For example, alloying Na^+ into $Cs_2AgInCl_6$ can efficiently break the parity-forbidden transition of the host material.[85]

Fourth, the preparation of dense and uniform high-quality thin films is a major challenge for almost all lead-free double perovskite detectors. For Bi^{3+}-based, Sn^{4+}-based, In^{3+}-based, and novel Au^{3+}-based, Sb^{3+}-based double perovskite, their precursor materials are mostly insoluble in organic solvents, thus making it difficult to obtain pure-phase films when preparing films by spin-coating method. We shoule explore more effective synthesis strategies to prepare high-quality lead-free double perovskite with optimized morphologies. Among them, proper post-thermal annealing treatment of spin-coated films is an effective option. In addition, using vacuum thermal evaporation to prepare double perovskite thin films is also feasible. For example, the self-powered UV photodetector, which based on $Cs_2AgBiBr_6$ thin film prepared by sequential vacuum evaporation method， has obtained a high on/off ratio of 6.6×10^3 and a fast response time of 6.13/28.02 μs.[79] In addition, the synthesis of pure-phase and large-size single crystals is also crucial for the development of lead-free double perovskite detectors. Compared with thin films, bulk single crystals display the advantages of less defects and high stability. For high formation energy Sb^{3+}-based double perovskite, the synthesis of pure phase single crystals remains to be explored. Accordingly, we should deepen our understanding of the crystallization mechanism involved in the synthesis process, which can help to improve the morphology of the films and single crystal, thus optimize the device performance.

Finally, for some double perovskites which have very weak or no PL emission, such as Fe^{3+}-based, Au^{3+}-based, and Ti^{4+}-based[86] double perovskites, we need to understand the possible reasons behind such as the indirect bandgap, and the parity forbidden direct/indirect transition, and then solve the problems using strategies such as doping , alloying and tailoring the dimensionality.

(2) The device performance needs to be further improved. The ideal photodetector should have excellent spectral response range tunability, high responsitivity, high sensitivity, low noise, and high stability. Looking into the future, research on how to improve the performance of lead-free double perovskite photodetectors can start from four aspects, including reducing dark current, increasing response speed, fabricating the wide-spectrum photodetector, andengineering the interface of the devices.

First, a lower dark current is a prerequisite for high detectivity. For semiconductor-based photodetectors, the dark current is closely related to the defect density of the materials. However, the crystal defects of lead-free double perovskite are much more numerous than those of lead-based perovskite. For example, the Bi_{Ag} and halogen vacancies in Bi^{3+}-based double perovskite and In_{Ag} in In^{3+} based double perovskite are deep electron traps, and these unnecessary deep-level defects strongly affect the carrier density and transport. In the meanwhile, the direct contact between the perovskite layer and the functional layer can cause interface recombination loss, and the combined effects of these factors will lead to a higher dark current in the device. Optimizing the growth conditions or metal ion doping can suppress internal defects in the crystal, while introducing a passivation layer on the surface of perovskite can eliminating the surface defects. These strategies can effectively reduce the dark current of the device and improve the detectivity. For example, doping Rb^+ in $Cs_2AgBiBr_6$ crystal can improve its response to X-rays due to the extended carrier lifetime, significant reduction of dark current and polarization formation.[87]

Second, in optical communication and time-of-flight imaging applications, the high response speed of detectors is essential. In theory, reducing the time required for carrier diffusion and charge collection helps to obtain high-speed photodetectors. When designing lead-free double perovskite-based photodetectors, the strategy of shortening the distance between electrodes can improve charge collection efficiency. For detectors with vertical structures, reducing the thickness of the semiconductor layer can achieve a rapid response of the device.

Third, the research of wide-spectrum photodetectors based on lead free double perovskite will be an important research field for future photodetectors. The narrow bandgap characteristic of perovskite is the primary condition for achieving wide spectral detection. The narrow band gap property of perovskite is the primary requirement for achieving broad-spectrum detection. For Sb^{3+}-based, Ti^{4+}-based, Fe^{3+}-based, Au^{3+}-based, and Sn^{4+}-based double perovskite, their bandgap is relatively small, making them suitable candidates for manufacturing wide spectral detectors. For Bi^{3+}-based, In^{3+}-based and other large bandgap double perovskite, energy band engineering is an effective way to adjust their bandgaps and design suitable carrier leap modes. Another commonly used strategy for achieving broadband detection (in the visible and near-infrared regions) is to integrate perovskite with low bandgap polymers or organic small molecules, such as $CyPF_6$, $Cy1BF_4$,[88] NDI-DPP,[89] PTB7-Th,[90] and so on. For example, a broadband detector can be fabricated by combining perovskite with low bandgap PDPPTDTPT, which shows a spectral response range of 350 nm to 1050 nm and an ultrafast response rate of 5 ns at a wavelength of 800 nm.[91]

Finally, to achieve high-performance photodetectors, interface engineering is needed to improve the charge separation and extraction rates.[92] In optoelectronic devices, solution-based prepared perovskite films have many pinholes and surface defects, and the perovskite materials are usually sensitive to the surface conditions of adjacent layers, which requires the introduction of appropriate insertion layers to alleviate the impact of these unfavorable factors on device performance.[93] Introducing functionalized interlayers can promote favorable interface charge dynamics and minimize carrier loss of interfacial dipoles, ultimately improving device performance. For example， F4-TCNQ layer (2,3,5,6-tetrafluoro-7,7,8,8-tetracyanoquinodimethane) was introduced between NiO_x/perovskite layers, and it can increase the hole concentration and work function of NiO_x HTL and thus can improve hole extraction and carrier mobility.[94] Functionalized interlayers, such as the ALD-MOx interlayer mentioned before, can also significantly optimize the quality of perovskite films. Besides, a suitable interface layer facilitates the ideal energy band alignment between the perovskite and the transport layers. Currently, the ETLs used for perovskite photodetectors are usually metal oxides such as ZnO, TiO_2, and SnO_2. However, at the ETL and perovskite interface, we usually observe non-radiative recombination and low electron extraction efficiency, so it is necessary to introduce an additional interface layer to alleviate these problems. For example, $ZrCl_4$ can modify the TiO_2 ETL by eliminating the offset between the conduction band edge of the TiO_2 transport layer and the absorber and improving the charge extraction efficiency, thus perovskite solar cells based on modified ETL achieved a much higher stable efficiency.[95] Regarding interface engineering, future research can focus on developing multifunctional molecular interface materials that can simultaneously passivate the defects, enhance the device carrier extraction, and extend the device lifetime.[96] We believe that the performance of lead-free double perovskite-based photodetectors will improve gradually and move closer to commercialization as more and more researchers are involved.

Based on the above discussions, although the performance of lead-free double perovskite photodetectors may be inferior to that of lead halide devices, there is no doubt that lead-free double perovskite has unlimited potential for applications in optoelectronic devices such as photodetectors.

With a deeper understanding of the fundamental physical and optical properties of lead-free double perovskite, we can completely achieve photodetector with stable performance, environmental friendliness, and high commercial value. The technology of lead-free perovskite photodetector is young and promising, and we believe that its development path will become more and more open and bright.

Author Contributions: Xiaoyan Li and Junzhe Shi wrote the original draft. Jianjun Chen，Zuojun Tan, and Hongwei Lei reviewed and edited the paper with constructive suggestions. All authors have read and agreed to the published version of the manuscript.

Acknowledgments: This work was financially supported by the Fundamental Research Funds for the Central Universities (Grant No. 2662023LXPY006), the National Natural Science Foundation of China (Grant No. 11904115), and the Open Foundation of Hubei Key Laboratory of Optical Information and Pattern Recognition, Wuhan Institute of Technology (Grant No. 202103).

Conflicts of Interest: The authors declare no conflict of interest.

Reference

1. Li J, Duan J, Yang X, et al. Review on recent progress of lead-free halide perovskites in optoelectronic applications[J]. Nano Energy, 2021, 80: 105526.
2. Akkerman Q A, Rainò G, Kovalenko M V, et al. Genesis, challenges and opportunities for colloidal lead halide perovskite nanocrystals[J]. Nature materials, 2018, 17(5): 394-405.
3. Zhang Z, Yang G, Zhou C, et al. Optical and electrical properties of all-inorganic Cs2AgBiBr6 double perovskite single crystals[J]. RSC advances, 2019, 9(41): 23459-23464.
4. Volonakis G, Haghighirad A A, Milot R L, et al. Cs2InAgCl6: a new lead-free halide double perovskite with direct band gap[J]. The journal of physical chemistry letters, 2017, 8(4): 772-778.
5. Singh A, Chaurasiya R, Bheemaraju A, et al. Strain-Induced Band-Edge Modulation in Lead-Free Antimony-Based Double Perovskite for Visible-Light Absorption[J]. ACS Applied Energy Materials, 2022, 5(4): 3926-3932.
6. Zhang L, Wang K, Zou B. Bismuth Halide Perovskite-Like Materials: Current Opportunities and Challenges[J]. ChemSusChem, 2019, 12(8): 1612-1630.
7. Longo G, Mahesh S, Buizza L R V, et al. Understanding the performance-limiting factors of Cs2AgBiBr6 double-perovskite solar cells[J]. ACS Energy Letters, 2020, 5(7): 2200-2207.
8. Lei L Z, Shi Z F, Li Y, et al. High-efficiency and air-stable photodetectors based on lead-free double perovskite Cs2AgBiBr6 thin films[J]. Journal of Materials Chemistry C, 2018, 6(30): 7982-7988.
9. Yan G, Jiang B, Yuan Y, et al. Importance of Bi–O Bonds at the Cs2AgBiBr6 Double-Perovskite/Substrate Interface for Crystal Quality and Photoelectric Performance[J]. ACS applied materials & interfaces, 2020, 12(5): 6064-6073.
10. Arora N, Dar M I, Hinderhofer A, et al. Perovskite solar cells with CuSCN hole extraction layers yield stabilized efficiencies greater than 20%[J]. Science, 2017, 358(6364): 768-771.
11. Qin P, Tanaka S, Ito S, et al. Inorganic hole conductor-based lead halide perovskite solar cells with 12.4% conversion efficiency[J]. Nature communications, 2014, 5(1): 3834.
12. Wijeyasinghe N, Regoutz A, Eisner F, et al. Copper(I) thiocyanate (CuSCN) hole-transport layers processed from aqueous precursor solutions and their application in thin-film transistors and highly efficient organic and organometal halide perovskite solar cells. Adv Funct Mater, 2017, 27: 1701818
13. Yan G, Ji Z, Li Z, et al. All-inorganic Cs2AgBiBr6/CuSCN-based photodetectors for weak light imaging[J]. Sci. China Mater., 2020.
14. Shen, Wenhu, et al. "Enhanced device performance of Cs2AgBiBr6 double perovskite photodetector by SnO2/ZnO double electron transport layer." Journal of Alloys and Compounds 929 (2022): 167329.
15. Lee H J, Na S I. Investigation of PCBM/ZnO and C60/BCP-based electron transport layer for high-performance pin perovskite solar cells[J]. Journal of Alloys and Compounds, 2022, 921: 166007.
16. Liu G, Zhong Y, Mao H, et al. Highly efficient and stable ZnO-based MA-free perovskite solar cells via overcoming interfacial mismatch and deprotonation reaction[J]. Chemical Engineering Journal, 2022, 431: 134235.
17. Ruankham P, Wongratanaphisan D, Gardchareon A, et al. Full coverage of perovskite layer onto ZnO nanorods via a modified sequential two-step deposition method for efficiency enhancement in perovskite solar cells[J]. Applied Surface Science, 2017, 410: 393-400.
18. Sivashanmugan K, Lin C H, Hsu S H, et al. Interfacial engineering of ZnO surface modified with poly-vinylpyrrolidone and p-aminobenzoic acid for high-performance perovskite solar cells[J]. Materials Chemistry and Physics, 2018, 219: 90-95.

19. Yang Z, Babu B H, Wu S, et al. Review on practical interface engineering of perovskite solar cells: From efficiency to stability[J]. Solar Rrl, 2020, 4(2): 1900257.
20. Niu H, Fang C, Wei X, et al. Magnetron sputtered ZnO electron transporting layers for high performance perovskite solar cells[J]. Dalton Transactions, 2021, 50(19): 6477-6487.
21. Yuan, Ye, et al. UV soaking for enhancing the photocurrent and response speed of Cs2AgBiBr6-based all-inorganic perovskite photodetectors. Science China Materials 65.2 (2022): 442-450.
22. Tress W, Yavari M, Domanski K, et al. Interpretation and evolution of open-circuit voltage, recombination, ideality factor and subgap defect states during reversible light-soaking and irreversible degradation of perovskite solar cells[J]. Energy & Environmental Science, 2018, 11(1): 151-165.
23. Yamada Y, Endo M, Wakamiya A, et al. Spontaneous defect annihilation in CH3NH3PbI3 thin films at room temperature revealed by time-resolved photoluminescence spectroscopy[J]. The journal of physical chemistry letters, 2015, 6(3): 482-486.
24. Tian Y, Merdasa A, Unger E, et al. Enhanced organo-metal halide perovskite photoluminescence from nanosized defect-free crystallites and emitting sites[J]. The Journal of Physical Chemistry Letters, 2015, 6(20): 4171-4177.
25. Tian Y, Peter M, Unger E, et al. Mechanistic insights into perovskite photoluminescence enhancement: light curing with oxygen can boost yield thousandfold[J]. Physical Chemistry Chemical Physics, 2015, 17(38): 24978-24987.
26. Chen S, Wen X, Huang S, et al. Light illumination induced photoluminescence enhancement and quenching in lead halide perovskite[J]. Solar Rrl, 2017, 1(1): 1600001.
27. Steele J A, Pan W, Martin C, et al. Photophysical pathways in highly sensitive Cs2AgBiBr6 double-perovskite single-crystal X-ray detectors[J]. Advanced Materials, 2018, 30(46): 1804450.
28. Xu Q, Shao W, Li Y, et al. High-sensitivity X-ray imaging of a lead halide perovskite single-crystal scintillator[J]. Optics Letters, 2020, 45(2): 355-358.
29. Douissard P A, Cecilia A, Rochet X, et al. A versatile indirect detector design for hard X-ray microimaging[J]. Journal of Instrumentation, 2012, 7(09): P09016.
30. Lian L, Zheng M, Zhang W, et al. Efficient and Reabsorption-Free Radioluminescence in Cs3Cu2I5 Nanocrystals with Self-Trapped Excitons[J]. Advanced Science, 2020, 7(11): 2000195.
31. Chen Q, Wu J, Ou X, et al. All-inorganic perovskite nanocrystal scintillators[J]. Nature, 2018, 561(7721): 88-93.
32. Zhang X, Yu S, Meng X, et al. A Review on Lead-Free Perovskites for X-Ray Detection and Imaging[J]. Crystal Research and Technology, 2023: 2200232.
33. Wu Y, Feng J, Yang Z, et al. Halide Perovskite: A Promising Candidate for Next-Generation X-Ray Detectors[J]. Advanced Science, 2023, 10(1): 2205536.
34. Yuan W, Niu G, Xian Y, et al. In situ regulating the order–disorder phase transition in Cs2AgBiBr6 single crystal toward the application in an X-ray detector[J]. Advanced Functional Materials, 2019, 29(20): 1900234.
35. Pan W, Wu H, Luo J, et al. Cs2AgBiBr6 single-crystal X-ray detectors with a low detection limit[J]. Nature photonics, 2017, 11(11): 726-732.
36. Steele J A, Pan W, Martin C, et al. Photophysical pathways in highly sensitive Cs2AgBiBr6 double-perovskite single-crystal X-ray detectors[J]. Advanced Materials, 2018, 30(46): 1804450.
37. Shao Q, Yan J, Gong W, et al. Dopant-compensated Cs2AgBiBr6−xClx single crystals for photo-imaging and X-ray detection[J]. Journal of Materials Chemistry C, 2022, 10(48): 18366-18374.
38. Tie S, Dong S, Yuan R, et al. Halide perovskites for sensitive, stable and scalable X-ray detection and imaging[J]. Chemical Communications, 2023.
39. Wang M, Zeng P, Bai S, et al. High-quality sequential-vapor-deposited Cs2AgBiBr6 thin films for lead-free perovskite solar cells[J]. Solar Rrl, 2018, 2(12): 1800217.
40. Yang B, Hong F, Chen J, et al. Colloidal Synthesis and Charge-Carrier Dynamics of Cs2AgSb1− yBiyX6 (X: Br, Cl; 0≤ y≤ 1) Double Perovskite Nanocrystals[J]. Angewandte Chemie, 2019, 131(8): 2300-2305.
41. Rodrigues J E F S, Escanhoela Jr C A, Fragoso B, et al. Experimental and theoretical investigations on the structural, electronic, and vibrational properties of Cs2AgSbCl6 double perovskite[J]. Industrial & Engineering Chemistry Research, 2021, 60(51): 18918-18928.
42. Wei F, Deng Z, Sun S, et al. Enhanced visible light absorption for lead-free double perovskite Cs2AgSbBr6[J]. Chemical Communications, 2019, 55(26): 3721-3724.
43. Wang C F, Li H, Ji Q, et al. Discovery of a 2D Hybrid Silver/Antimony-Based Iodide Double Perovskite Photoferroelectric with Photostrictive Effect and Efficient X-Ray Response[J]. Advanced Functional Materials, 2022, 32(40): 2205918.
44. Yin H, Xian Y, Zhang Y, et al. An Emerging Lead-Free Double-Perovskite Cs2AgFeCl6: In Single Crystal[J]. Advanced Functional Materials, 2020, 30(43): 2002225.
45. Volonakis G, Haghighirad A A, Milot R L, et al. Cs2InAgCl6: a new lead-free halide double perovskite with direct band gap[J]. The journal of physical chemistry letters, 2017, 8(4): 772-778.

46. Luo J, Li S, Wu H, et al. Cs2AgInCl6 double perovskite single crystals: parity forbidden transitions and their application for sensitive and fast UV photodetectors[J]. Acs Photonics, 2018, 5(2): 398-405.
47. Liao Q, Chen J, Zhou L, et al. Bandgap engineering of lead-free double perovskite Cs2AgInCl6 nanocrystals via Cu2+-doping[J]. The Journal of Physical Chemistry Letters, 2020, 11(19): 8392-8398.
48. Locardi F, Cirignano M, Baranov D, et al. Colloidal synthesis of double perovskite Cs2AgInCl6 and Mn-doped Cs2AgInCl6 nanocrystals[J]. Journal of the American Chemical Society, 2018, 140(40): 12989-12995.
49. Jia H, Zhang X, Feng Z, et al. Na+-doped lead-free double perovskite Cs2AgInCl6 for broadband solar-blind UV detection[J]. Optical Materials, 2022, 128: 112365.
50. Slavney A H, Leppert L, Saldivar Valdes A, et al. Small-band-gap halide double perovskites[J]. Angewandte Chemie, 2018, 130(39): 12947-12952.
51. Roy M, Borkar H, Alam A, et al. Spontaneous anion-exchange synthesis of optically active mixed-valence Cs2Au2I6 perovskites from layered CsAuCl4 perovskites[J]. Chemical Communications, 2021, 57(12): 1478-1481.
52. Kangsabanik J, Ghorui S, Aslam M, et al. Optoelectronic Properties and Defect Physics of Lead-Free Photovoltaic Absorbers Cs2AuIAuIIIX6 (X= I, Br)[J]. Physical Review Applied, 2020, 13(1): 014005.
53. Ghosh B, Febriansyah B, Harikesh P C, et al. Direct Band Gap Mixed-Valence Organic–inorganic Gold Perovskite as Visible Light Absorbers[J]. Chemistry of Materials, 2020, 32(15): 6318-6325.
54. Stoumpos C C, Malliakas C D, Kanatzidis M G. Semiconducting tin and lead iodide perovskites with organic cations: phase transitions, high mobilities, and near-infrared photoluminescent properties[J]. Inorganic chemistry, 2013, 52(15): 9019-9038.
55. Leijtens T, Prasanna R, Gold-Parker A, et al. Mechanism of tin oxidation and stabilization by lead substitution in tin halide perovskites[J]. ACS Energy Letters, 2017, 2(9): 2159-2165.
56. Han X, Liang J, Yang J H, et al. Lead-free double perovskite Cs2SnX6: facile solution synthesis and excellent stability[J]. Small, 2019, 15(39): 1901650.
57. Ullah S, Wang J, Yang P, et al. Lead-Free Cs2SnI6 Perovskites for Optoelectronic Applications: Recent Developments and Perspectives[J]. Solar RRL, 2021, 5(5): 2000830.
58. Krishnaiah M, Khan M M I, Kumar A, et al. Impact of CsI concentration, relative humidity, and annealing temperature on lead-free Cs2SnI6 perovskites: Toward visible light photodetectors application[J]. Materials Letters, 2020, 269: 127675.
59. Huang J, Dong C, Mei Y, et al. The precursor-compensation strategy boosts the photoresponse performance of air-stable, self-powered Cs2SnI6 photodetectors[J]. Journal of Materials Chemistry C, 2021, 9(40): 14217-14225.
60. Shen J, Zhu W, Lian Z, et al. Metal Ion-Incorporated Lead-Free Perovskites toward Broadband Photodetectors[J]. ACS Applied Electronic Materials, 2023.
61. Ye X, Liu A, Gao L, et al. Computational screening of Cs based vacancy-ordered double perovskites for solar cell and photocatalysis applications[J]. EcoMat, 2022: e12295.
62. Nouri Y, Hartiti B, Batan A, et al. The structural, mechanical, thermal, electronic and optical properties of halide perovskites Cs2TiX6 (X= Cl, Br, I): First-principles investigations[J]. Solid State Communications, 2023: 115087.
63. Chen M, Ju M G, Carl A D, et al. Cesium titanium (IV) bromide thin films based stable lead-free perovskite solar cells[J]. Joule, 2018, 2(3): 558-570.
64. Ju D, Zheng X, Yin J, et al. Tellurium-based double perovskites A2TeX6 with tunable band gap and long carrier diffusion length for optoelectronic applications[J]. ACS Energy Letters, 2018, 4(1): 228-234.
65. Yoshihiro F, Hideko K, Ryuichi I. Molecular motion in methylammonium hexahalotellurates (IV) as studied by means of the pulsed nuclear magnetic resonance[J]. Bulletin of the Chemical Society of Japan, 1981, 54(1): 103-108.
66. Guo J, Xu Y, Yang W, et al. High-stability flexible X-ray detectors based on lead-free halide perovskite Cs2TeI6 films[J]. ACS Applied Materials & Interfaces, 2021, 13(20): 23928-23935.
67. Zhao P, Su J, Guo Y, et al. A new all-inorganic vacancy-ordered double perovskite Cs2CrI6 for high-performance photovoltaic cells and alpha-particle detection in space environment[J]. Materials Today Physics, 2021, 20: 100446.
68. Dong Q, Fang Y, Shao Y, et al. Electron-hole diffusion lengths> 175 μm in solution-grown CH3NH3PbI3 single crystals[J]. Science, 2015, 347(6225): 967-970.
69. Ye F, Lin H, Wu H, et al. High-quality cuboid CH3NH3PbI3 single crystals for high performance X-ray and photon detectors[J]. Advanced Functional Materials, 2019, 29(6): 1806984.
70. Hooijer R, Weis A, Biewald A, et al. Silver-Bismuth Based 2D Double Perovskites (4FPEA)4AgBiX8 (X= Cl, Br, I): Highly Oriented Thin Films with Large Domain Sizes and Ultrafast Charge-Carrier Localization[J]. Advanced Optical Materials, 2022, 10(14): 2200354.
71. Wu C, Du B, Luo W, et al. Highly efficient and stable self-powered ultraviolet and deep-blue photodetector based on Cs2AgBiBr6/SnO2 heterojunction[J]. Advanced Optical Materials, 2018, 6(22): 1800811.

72. Yang J, Bao C, Ning W, et al. Stable, high-sensitivity and fast-response photodetectors based on lead-free Cs2AgBiBr6 double perovskite films[J]. Advanced Optical Materials, 2019, 7(13): 1801732.
73. Li Y, Shi Z, Liang W, et al. Recent advances toward environment-friendly photodetectors based on lead-free metal halide perovskites and perovskite derivatives[J]. Materials Horizons, 2021, 8(5): 1367-1389.
74. Shao D, Zhu W, Xin G, et al. Inorganic vacancy-ordered perovskite Cs2SnCl6: Bi/GaN heterojunction photodiode for narrowband, visible-blind UV detection[J]. Applied Physics Letters, 2019, 115(12): 121106.
75. Li Y, Shi Z, Lei L, et al. Ultrastable lead-free double perovskite photodetectors with imaging capability[J]. Advanced Materials Interfaces, 2019, 6(10): 1900188.
76. Lai Z, Wang F, Meng Y, et al. Solution-processed lead-free double perovskite microplatelets with enhanced photoresponse and thermal stability[J]. Sci. China Mater, 2022, 65: 1313-1319.
77. Sakai N, Haghighirad A A, Filip M R, et al. Solution-processed cesium hexabromopalladate (IV), Cs2PdBr6, for optoelectronic applications[J]. Journal of the American Chemical Society, 2017, 139(17): 6030-6033.
78. Shuang Z, Zhou H, Wu D, et al. Low-temperature process for self-powered lead-free Cs2AgBiBr6 perovskite photodetector with high detectivity[J]. Chemical Engineering Journal, 2022, 433: 134544.
79. Zhang X, Liu X, Sun B, et al. Ultrafast, self-powered, and charge-transport-layer-free ultraviolet photodetectors based on sequentially vacuum-evaporated lead-free Cs2AgBiBr6 thin films[J]. ACS Applied Materials & Interfaces, 2021, 13(30): 35949-35960.
80. Lee J W, Bae S H, Hsieh Y T, et al. A bifunctional lewis base additive for microscopic homogeneity in perovskite solar cells[J]. Chem, 2017, 3(2): 290-302.
81. Ji F, Boschloo G, Wang F, et al. Challenges and Progress in Lead-Free Halide Double Perovskite Solar Cells[J]. Solar RRL, 2023: 2201112.
82. Lei H, Hardy D, Gao F. Lead-free double perovskite Cs2AgBiBr6: fundamentals, applications, and perspectives[J]. Advanced Functional Materials, 2021, 31(49): 2105898.
83. Fang Y, Zhang L, Wu L, et al. Pressure-induced emission (PIE) and phase transition of a two-dimensional halide double perovskite (BA)4AgBiBr8 (BA=CH3(CH2)3NH3+)[J]. Angewandte Chemie International Edition, 2019, 58(43): 15249-15253.
84. Yao Y, Kou B, Peng Y, et al. (C3H9NI)4AgBiI8: a direct-bandgap layered double perovskite based on a short-chain spacer cation for light absorption[J]. Chemical Communications, 2020, 56(21): 3206-3209.
85. Luo J, Wang X, Li S, et al. Efficient and stable emission of warm-white light from lead-free halide double perovskites[J]. Nature, 2018, 563(7732): 541-545.
86. Euvrard J, Wang X, Li T, et al. Is Cs2TiBr6 a promising Pb-free perovskite for solar energy applications?[J]. Journal of Materials Chemistry A, 2020, 8(7): 4049-4054.
87. Keshavarz M, Debroye E, Ottesen M, et al. Tuning the Structural and Optoelectronic Properties of Cs2AgBiBr6 Double-Perovskite Single Crystals through Alkali-Metal Substitution[J]. Advanced Materials, 2020, 32(40): 2001878.
88. Lin Q, Wang Z, Young M, et al. Near-Infrared and Short-Wavelength Infrared Photodiodes Based on Dye–Perovskite Composites[J]. Advanced Functional Materials, 2017, 27(38): 1702485.
89. Xu W, Guo Y, Zhang X, et al. Room-temperature-operated ultrasensitive broadband photodetectors by perovskite incorporated with conjugated polymer and single-wall carbon nanotubes[J]. Advanced Functional Materials, 2018, 28(7): 1705541.
90. Wu G, Fu R, Chen J, et al. Perovskite/Organic Bulk-Heterojunction Integrated Ultrasensitive Broadband Photodetectors with High Near-Infrared External Quantum Efficiency over 70%[J]. Small, 2018, 14(39): 1802349.
91. Shen L, Lin Y, Bao C, et al. Integration of perovskite and polymer photoactive layers to produce ultrafast response, ultraviolet-to-near-infrared, sensitive photodetectors[J]. Materials Horizons, 2017, 4(2): 242-248.
92. Mak C H, Huang X, Liu R, et al. Recent progress in surface modification and interfacial engineering for high-performance perovskite light-emitting diodes[J]. Nano Energy, 2020, 73: 104752.
93. Wu Y, Wang D, Liu J, et al. Review of interface passivation of perovskite layer[J]. Nanomaterials, 2021, 11(3): 775.
94. Yang J, Wang Y, Huang L, et al. High-Efficiency and Stable Perovskite Photodetectors with an F4-TCNQ-Modified Interface of NiOx and Perovskite Layers[J]. The Journal of Physical Chemistry Letters, 2022, 13(17): 3904-3914.
95. Gkini K, Orfanoudakis S, Tsipas P, et al. ZrCl4 for energy level alignment at the perovskite/TiO2 interface[J]. Electrochimica Acta, 2022, 433: 141214.
96. Li Y, Xie H, Lim E L, et al. Recent progress of critical interface engineering for highly efficient and stable perovskite solar cells[J]. Advanced Energy Materials, 2022, 12(5): 2102730.